Atmósfera (1991), **4**, *pp. 205-233*

Radiative properties of cirrus clouds

P. P. ANIKIN, E. M. FEIGELSON, I. A. GORCHAKOVA, T. A. TARASOVA
Institute of Atmospheric Physics, USSR Academy of Sciences

L. V. KRAVETS, N. A. ZAYTSEVA
Central Aerological Observatory, USSR, State Committee for Hydrometeorology

G. M. ABAKUMOVA, E. I. NESVAL, T. B. YEVNEVICH
Moscow State University

T. A. TOCHILKINA
Moscow Instrument Making Institute

A. G. PETRUSHIN
Institute of Experimental Meteorology, State Committee for Hydrometeorology

(Manuscript received June 6, 1990; accepted in final form Jan. 25, 1991)

RESUMEN

Se presentan resultados basados en observaciones de superficie para estudiar altura, grosor, propiedades ópticas de nubes cirrus y flujos radiativos.

Se describen estudios teóricos relativos a algunos efectos de difracción, problemas de inversión de sondeos lidar, y construcción de modelos ópticos de nubes cirrus. Se llevan a cabo cálculos de flujos de radiación solar y termal, albedo y balances radiativos, comparando los resultados con datos experimentales.

ABSTRACT

Results are presented of a ground based experiment for studying heights, thicknesses, optical properties of cirrus clouds and radiative fluxes.

Theoretical studies concerning some diffraction effects, inverse problems of lidar sounding, and construction of optical models of cirrus clouds are described. Calculations of fluxes of solar and thermal radiation, albedo, and radiative balances are performed and compared with experimental data.

Introduction

In May 1986-1987 at the Zvenigorod scientific station (ZSS) of the Institute of Atmospheric Physics (USSR Academy of Sciences) a comprehensive ground-based experiment was conducted for studying the optical and radiative properties of cirrus clouds.

The following measurements were made: spectral transmission of solar radiation; levels of the cloud boundaries; vertical profiles of the scattering coefficient; emittance in the "window" of 8 - 12 μm; fluxes of spectral and integral solar radiation-direct, diffuse and global; temperature and

humidity near the surface; estimates of clouds ice content. Use was made of aerological data in the town "Dolgoprudny" located 80 km away from the town "Zvenigorod".

Theoretical studies and calculations of radiative fluxes were carried out, based and compared with the experimental data.

A detailed description of the results of experimental and theoretical studies, along with reviews of the climatology, microphysics and optics of cirrus clouds, are given in the collection "Radiative Properties of Cirrus Clouds". Edited by E. M. Feigelson. Nauka Publishers, Moscow, 1989.

Part I. Experimental results and their interpretation

1. Spectral transmission and optical thicknesses

To measure the spectral transmissions of cirrus clouds-P_λ, use was made of an optical device which made it possible to carry out simultaneous determinations of P_λ in five sections of the spectrum: 0.3-0.5 μm; 0.32-0.8 μm; 0.4-1.2 μm; 0.5-2.2 μm; 2-12 μm. The direct solar radiation I_λ was recorded simultaneously by five spectrometers with resolutions: $\Delta\lambda = 10^{-3}$ μm when $\lambda \leq 1.2$ μm and $\Delta\lambda = 4.10^{-2}$ μm when $\lambda \geq 3.9$ μm. The solar radiation flux was directed into the device by a special Sun tracking unit. Using a system of mirrors and semitransparent quartz plates, a portion of the flux was directed on spectrometers which were tuned in to $\lambda = 0.31$; 0.63; 1.2; 2.1; 10.2 μm. The angle of view of the device $\alpha = 15$ minutes. The device is described in detail in Anikin *et al.* (1981).

The spectral transmission P_λ of cirrus clouds was determined from the following relation:

$$P_\lambda = I_\lambda / I_\lambda^o \tag{I.1}$$

where I_λ and I_λ^o are relative values of the direct solar radiation which pases through clouds and in breaks between them.

Then the transparency and optical thickness in the direction towards the zenith was determined:

$$P_\lambda^o = P_\lambda^{\cos\theta}; \quad \tau_\lambda = -lnP_\lambda^o \tag{I.2}$$

where θ the Sun's zenith angle. The values of τ_λ in the range $\tau_\lambda \leq 2$ were determined with a relative error of 5% which is mainly due to the inaccuracy in detecting the transmission when the sky is clear.

During the 1986-1987 experiment the data of τ_λ with $\lambda = 10.2$ μm were mainly processed. In the UV and visible spectral regions, along with the useful signal, i.e., direct solar light, a portion of scattered light (the greater portion the lower λ is) gets into the receiver even with a small angle of view, due to the diffraction effect of large crystals in cirrus clouds. As a result, the measured value of P_λ increases while τ_λ decreases. Figure I.1 gives an example of the spectral dependence of $\tau_\lambda/\tau_{\lambda_o}(\lambda_o = 10.2$ μm).

We have calculated this effect for the models of ice based on spherical particles of different effective radii in the wavelength range $\lambda = 0.6 - 10$ μm at the receiver's angles of view α, ranging from 15 minutes to 10 degrees. The results of calculations are presented in Figure I.2. Here $\overline{\tau}_\lambda$ is the optical thickness of the cloud with the contribution of scattered radiation getting into the

angle of the receiver's opening. τ_λ is the same for true direct radiation. It follows from Figure I.2 that in the visible range of the spectrum even at $\alpha = 15$ minutes for large particles the value $\overline{\tau}_\lambda/\tau_\lambda$ is much smaller than 1. With the growth of λ the deviation of $\overline{\tau}_\lambda/\tau_\lambda$ from unity with the same size of particles becomes smaller, which indicates the decrease of the share of scattered radiation in the measured signal. With $\lambda = 10$ μm $\overline{\tau}_\lambda/\tau_\lambda = 1$ in the entire range of particle sizes of interest. This was the main reason of the selection of the wavelength $\lambda - 10.2$ μm in determining τ_{λ_o}.

The measured value of τ_{λ_o} directly corresponds to emissivity measured in the transparency window of 8-12 μm:

$$\varepsilon = 1 - e^{-\tau_{\lambda_o}} \tag{I.3}$$

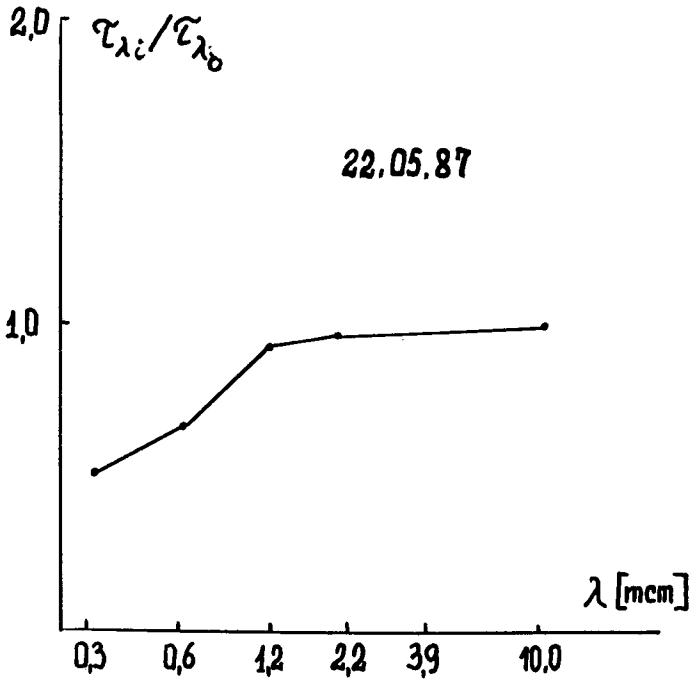

Fig. I. 1. The spectral dependence of optical thicknesses $\tau_{\lambda_i}/\tau_{\lambda_o}$ $\lambda_o = 10.2$ μm for the cirrus cloud of May 22, 1987.

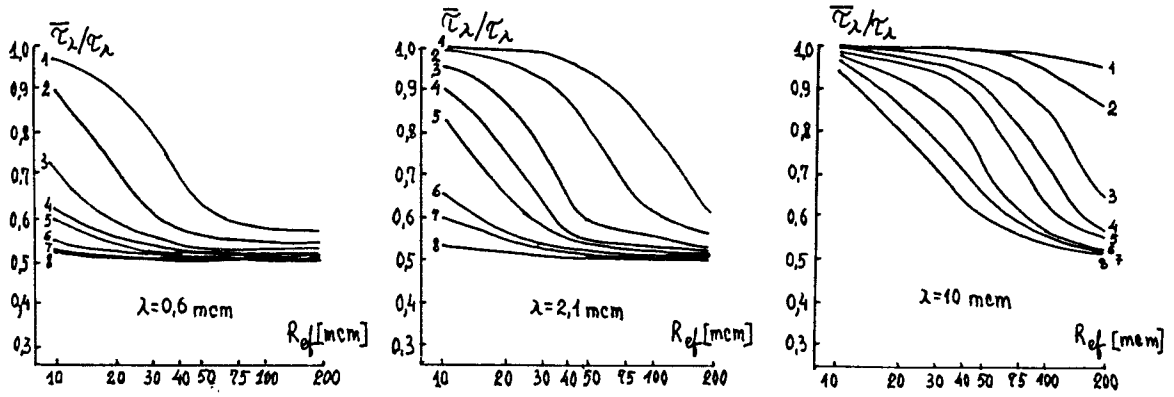

Fig. I. 2. The ratio of optical thicknesses $\overline{\tau}_\lambda/\tau_\lambda$ as a function of the effective radius of particles for the receiver's different angles of view α (1-15 minutes; 2-8: 1, 2, 3, 4, 6, 8, 10 degrees).

Finally, ignoring in the present stage of theoretical studies the effect of small particles, it can be assumed for solar and thermal radiation that $\tau_\lambda = \text{const} = \tau_{\lambda_o}$, $\lambda_o = 10.2$ μm.

The comparison of measured data by an integral actinometer with the angle of view $\alpha = 10$ degrees and our installation ($\alpha = 15$ minutes, $\lambda_o = 10.2$ μm) is a convincing confirmation of the data of Figure I.2. The results of simultaneous measurements presented on Figure I.3 show that the ratio $\tau_A/\tau_{\lambda_o} = 0.5$ is fulfilled practically exactly.

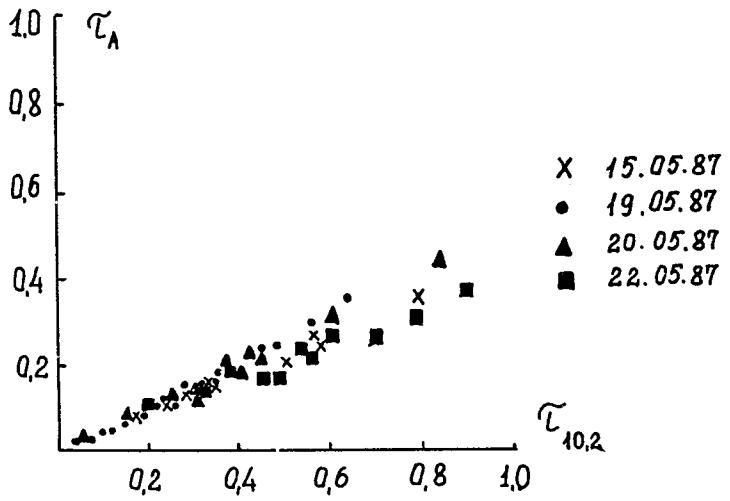

Fig. I. 3. Correlation between broadband optical thicknesses τ_A and τ at 10.2 μm for various days during the 1987 experiment.

Histograms of the recurrence of values $P^o_{\lambda_o}$ for cirrus during the years of study, as well as the averaged histogram for the 1978-1987 period are shown in Figure I.4. The overall time of observations is 89 hours.

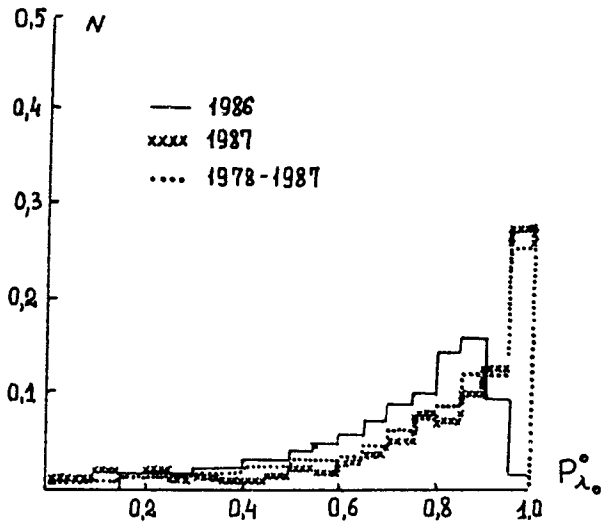

Fig. I. 4. Histograms of the recurrence frequencies of the transparency of cirrus clouds in the direction towards the zenith - $N(P_{\lambda_o})$ during the 1978-1987 period.

Table I.1 lists average values of τ_{λ_o} for a day, dispersions G_p^2 and time intervals - Δt for which autocorrelation coefficients were ≥ 0.7. The number of individual measurements not less than 1000 per day. It is evident in Figure I.4 and Table I.1 that cirrus clouds observed at the ZSS are mainly thin, semitransparent and variable clouds. As will be shown further such thin clouds give an essential greenhouse effect.

Table I. 1. Mean values of τ_{λ_o} for single days: dispersion - G_p^2 and time intervals -Δt for autocorrelation coefficients larger than 0.7.

Date:	11.05	24.05	04.05	06.05	15.05	19.05	20.05	22.05
Year:	1986				1987			
τ_{λ_o}	0.83	0.64	0.95	0.83	0.54	0.85	0.74	0.80
G_p^2	0.002	0.018	0.001	0.005	0.043	0.011	0.020	0.007
Δt_{sec}	55	90	17	65	140	72	120	120

2. Studies of cirrus clouds by a ground-based lidar

The lidar consists of a transmitter and a receiving aerial directed towards the zenith and separated from each other by 4 m. The transmitter uses a neodymium glass laser with a doubled radiation frequency. The receiver's angle of view was roughly equal to the divergence angle of the transmitter's beam (3 mrad). Table I.2 lists the main parameters of the lidar used, as compared with the parameters of the lidar described in Platt *et al.* (1987).

Table I.2. Lidars' parameters

	Wave-length	Pulse energy	Pulse dura-tion	Trans-mitter's angle	Receiv-er's angle	Aerial diameter
CAO lidar (glass + Nd)	1060 nm 530 nm	10 J 1.5 J	30 ns	3 mrad	3 mrad	50 cm
Lidar Platt at all	694 nm	1 J	60 ns	2 mrad	5 mrad	30 cm

The lidar's high energy potential enabled the reliable recording of cirrus clouds at any time of the day.

The lidar was used to determine the heights of cloud boundaries and for the retrieval of the vertical profile of the scattering coefficient at $\lambda = 530$ nm.

Cloud boundaries were determined from the threshold values of the backscattering coefficient $\beta_{\pi,\min}(Z)$. The latter is obtained by comparing measured signals from cirrus clouds with signals of daytime clear sky entering the recording instrumentation. The threshold values are listed in Table I.3.

Table I.3. Threshold values of β_π as functions of height H.

Height		6-7 km	8-9 km	10-11 km
$\beta_{\pi,\min}$	λ=1060 nm	$2\ 10^{-3}$	$3\ 10^{-3}$	$4\ 10^{-10}$
(km^{-1})	λ=530 nm	$5\ 10^{-3}$	$7.5\ 10^{-3}$	10^{-2}

The experience with this lidar has shown that the accuracy in determining the boundaries of cirrus clouds during measurements in the daytime is higher when $\lambda = 1060$ nm.

This method of determining the boundaries of thin clouds is conventional enough. Aerosol fluctuations and therefore aerosol backscattering coefficients greater than those taken as thresholds for clouds are possible. Nevertheless, as a rule, cirrus clouds with optical thicknesses $\tau > 0.1$ have values β_π which exceed ten or more times threshold values. This enables the differentiation of them from aerosol layers.

To retrieve the profiles of the scattering coefficient $\beta(Z)$ of the cloud from the measured profile of the lidar echo signal $-S(Z)$, we need the solution of the inverse problem. We have worked out the technique which includes, in addition to the measurements of the profile of the signal $S(Z)$, the measurements of the optical thickness of the cloud $-\tau$ (see section 1).

The technique is based on a modified method of successive layers MSL which gives a recurrence equation for values $\beta(\Delta Z_i)$ and $\beta(\Delta Z_{i+1})$ for neighbouring layers ΔZ_i and ΔZ_{i+1} (Zuyev *et al.*, 176).

$$\beta(\Delta Z_{i+1}) = \beta(\Delta Z_i) T^{-2}(\Delta Z_i) \frac{S(\Delta Z_{i+1})}{S(\Delta Z_i)} \tag{I.4}$$

where $T^2(\Delta Z_i) = \exp(-2\beta(\Delta Z_i)\Delta Z_i)$

In deriving (I.4) a slight change in height of the backscattering phase function $\gamma_\pi(Z)$ in the cloud is suggested as compared with the change of $\beta(Z)$. In the presence of the altitude profile of $S(Z)$ we propose the following algorithm to determine the function $\beta(Z)$:

1. a certain value of $\beta(\Delta Z_k)$ for the *kth* layer is given *a priori* when $1 < K < N$ (the layer K is chosen closer to the upper boundary, so that the value would be large enough, which leads to a smaller error);
2. with the help of formula (I.4) the profile $\beta(\Delta Z_I)$ is successively calculated.

Then a comparison is made of the calculated optical thickness $\tau_o = \sum_{i=1}^{N} \beta(\Delta Z_i) \cdot \Delta Z_i$ and the measured one $-\tau$. If the condition $\tau_o = \tau$ is not fulfilled, the value of the parameter $\beta(\Delta Z_k)$ varies, and the process is repeated until the last condition is fulfilled. As a result, we obtain the profile of the scattering coefficient $-\beta(\Delta Z_i)$.

The numerical experiment carried out in Zuyev *et al.* (1976) shows that in the entire range of optical thicknesses $\tau < 4$ even at the reception angle $\alpha = 1^\circ$ the deviation $\Delta\beta/\beta$ due to the multiple scattering background did not exceed 10%. We have conducted a numerical experiment to determine the effect of the changes of the backscattering phase function $-\gamma_\pi$ along the height

of the cloud in the accuracy of the retrieved $\beta(Z)$. In this experiment we also studied the effect of the error in the determination of the optical thickness τ, on the accuracy of the retrieval of the $\beta(Z)$ profile by the proposed method.

The effect of the change of the optical thickness τ on error in reconstructing the $\beta(Z)$ profile is more essential than the change of γ_π. The qualitative character of the $\beta(Z)$ is traced and for the greater part of the profile the coincidences between the reconstructed and original profiles are accurate enough. Thus, the suggested technique makes it possible to reliably reconstruct the profiles of the scattering coefficient in cirrus clouds. The practical value of the method consists in using only experimental information for solving the lidar equation. Besides, the calibration of the lidar is not needed.

The measurements were made for all high clouds in the altitude range of 5.5 - 12 km. The general character of the altitude distribution is given by histograms presented in Figure I.5. In May 1986 mainly thin cirrus clouds were observed. The average thickness for the entire measuring cycle was 600 m. In May 1987 thicker high clouds were observed; the average thickness for the cycle was 1000 m. The optical thicknesses varied within $0.1 \leq \tau \leq 1.2$.

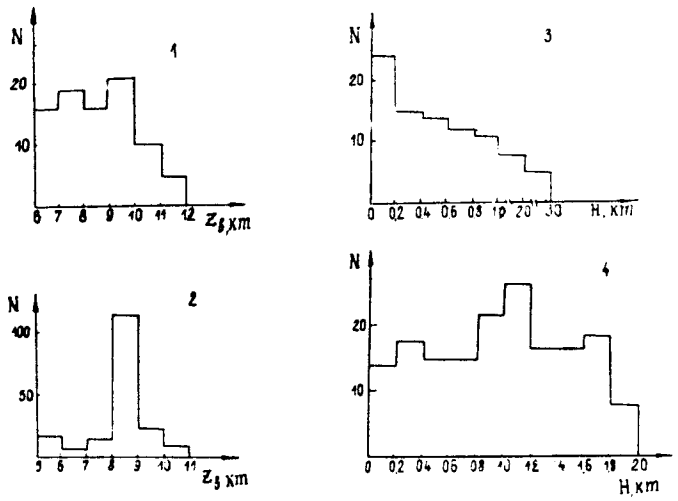

Fig. I. 5. Histograms of the heights of the lower boundary Z_b - 1, 2 and thicknesses of clouds - H - 3, 4 (1;3 - May 1986; 2;4 - May 1987) N - number of cases.

For the entire set of reconstructed profiles of the scattering coefficient $\beta(Z)$ for $\lambda = 0.53$ μm it was obtained that, as a rule, the maximum value of $\beta(Z)$ lies within the limits 0.4-1.2 km^{-1}. The absolute maximum of the obtained values of $\beta(Z)$ lay at a height of 6.7 km and was equal to 2.4 km^{-1}. The average in profile values of $\beta(Z)$ lie within the limits of 0.15-0.8 km^{-1}. Using the obtained data, we calculated the average relative profile $\beta(Z)$ represented in Figure I.6 for clouds whose thickness was close to 1 km, and the height of the lower boundary lays within 7.5-9 km. It can be concluded that the average profile of the distribution of $\beta(Z)$ in the given height interval has a weakly pronounced domeshaped maximum slightly shifted towards the upper boundary $-Z_t$. "Instantaneous" profiles for which the averaging was carried out had various shapes, including the two-humped shape with maxima near the lower and upper boundaries. The measured thicknesses of cirrus clouds are compared with the average scattering coefficient $< \beta >$ in Figure I.7 for clouds with $7.5 \leq Z_b \leq 9$ km.

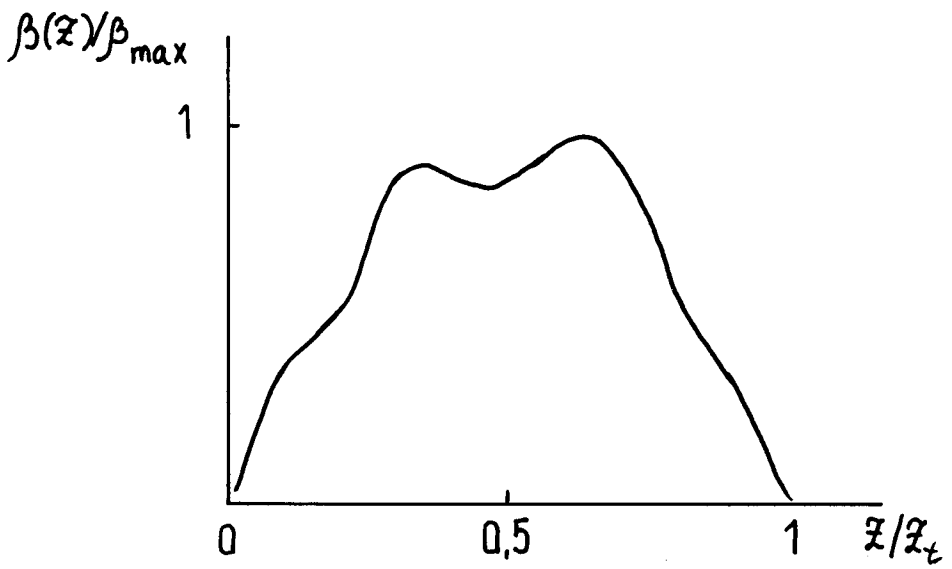

Fig. I. 6. The average profile of the distribution of $\beta(Z)/\beta_{max}$.

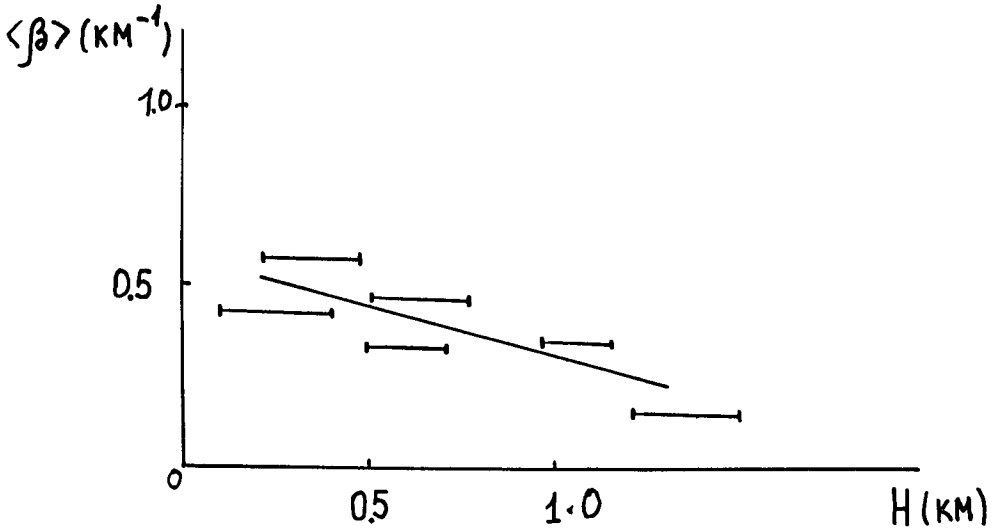

Fig. I. 7. Dependence of the average value of the scattering coefficient on the thickness of the cloud.

The comparisons of the thicknesses of observed cirrus clouds with the temperature t° at the middle of the cloud did not lead to obvious regular features. For instance, in the statistically most significative case the thicknesses of clouds for the temperature interval $-45^\circ C < t^\circ < -40^\circ C$ varied from 0.4 to 1.8 km.

3. Emissivity

The emissivity $-\varepsilon$ of cirrus clouds was measured by an IR-Radiometer which has the following technical characteristics: spectral range of operation 8-12 μm, angle of view 1°, sensitivity 0.1 K at the blackbody temperature of 283 K, time constant 1 sec.

Measurements were conducted in the direction towards the zenith.

The emissivity of cirrus clouds from the data of an IR-radiometer and a lidar was determined according to the formula (Zhuravlyova *et al.*, 1983).

$$\varepsilon = \frac{L_{cl}}{B(T)}; \; L_{cl} = \frac{L_m - L_{uc}}{P} - L_r \tag{1.5}$$

where ε - emissivity of the cloud; $B(T)$ - blackbody emission at the temperature of the lower boundary; L_{cl} - cloud's own emission; L_m - emission measured near the Earth's surface; L_{uc} - emission of the subcloud layer; L_r - Earth's emission reflected from the cloud; P - the transmission of the undercloud layer.

In our case $L_m - L_{uc}$ is determined as a difference between the emissions of the cloudy and the clear sky. We ignore the emission of the above-cloud layer, and $B(T)$ is determined on the basis of aerological data and lidar data of the height of the lower boundary.

According to experimental data the emissivity during the period of measurements in 1986-1987 varied from 0.1 to 0.99. Figure I.8. presents hystograms for these periods. Table I.4. lists mean values of ε, their dispersions - G_ε and the mean ice content - m_w^* for different days and hours of measurements.

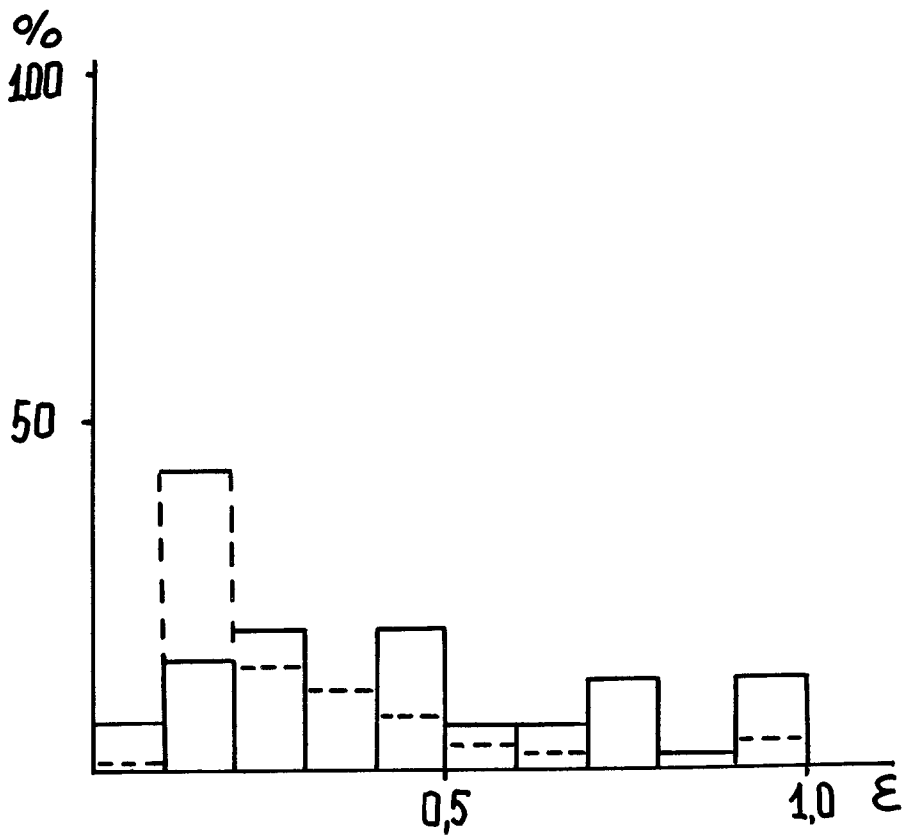

Fig. I. 8. Histograms of emissivity during the experiment. Solid line - results of 1986; Dashed line - results of 1987.

Table I.4. Emissivity and ice content of cirrus clouds.

Date time, hours	Mean emissivity	Dispersion G_ε	Mean ice content M_w g/m^2
10.05.86			
13-14, 15-16	0.46	0.031	48.0
14-15	0.66	0.026	61.5
4.05.87			
14-15	0.37	0.020	23.3
15-16	0.25	0.085	12.9
16-18	0.14	0.04	7.0
19.05.87			
14-15	0.15	0.01	8.34
15-18	0.29	0.012	15.0
20.05.87			
11-13	0.22	0.013	12.0
22.05.87			
11-13	0.27	0.013	15.0

The ice content was determined from the expression;

$$m_w = \rho r \tau_{cl} \tag{I.5}$$

where $\tau_{cl} = ln\frac{1}{1-\varepsilon}$; $\rho - 0.9$ g/cm^3; r - effective radius ≈ 50 μm. (Zhuravlyova and Kostko, 1986).

4. Solar spectral radiation at the surface

Direct integral solar radiation (I) was measured by a thermoelectric actinometer whose angle of view is equal to 10 degrees. The set of wideband lihgt filters made it possible to determine the value of direct radiation in spectral regions $\lambda < 525$ nm, 380 - 710 nm and $\lambda > 710$ nm.

Global (Q) and diffuse (D) integral radiation (int) were measured by a thermoelectric pyranometer; photosynthetically active radiation (par, 380-710 nm) and near infrared (nir, $\lambda > 710$ nm) radiation were measured by colour MGO* pyranometers, while ultraviolet radiation (uv, $\lambda < 380$ nm) was measured by an u.v. meter of Moscow University. The angle of view of these instruments was 180°. In measurements of diffuse radiation the devices were shaded to exclude the near-solar zone 10° in diameter equal to the actinometer's angle of view. The relative error of measurements by the actinometer was equal to 3% and by other devices to 11%.

When the sky was clear or the cirrus cloud cover was solid, observations of direct and diffuse radiation were conducted not rare than in half an hour. Global radiation (int, par, uv) was recorded continuously. Q nir = Q int - Q par - Q uv.

a. Direct solar radiation. The effect of cloudiness was calculated by equations I.1-2 for each spectral interval $\Delta\lambda$ mentioned above.

$I^o_{\Delta\lambda}$ was determined either from measurements in breaks between clouds or from measurements on a day close to the cloudy day with a similar synoptic situation.

* Main Geophysical Observatory.

Values of $P^o_{\Delta\lambda}$ and $\tau_{\Delta\lambda}$ averaged over the types of cirrus clouds are listed in Table I.5.

Direct radiation is most considerably attenuated by cirrus-stratus (Cs) clouds. Transmissions and the optical thicknesses of cirrus (Ci) and cirrus-cumulus (Cc) clouds are close to each other.

On average, the attenuation of $I_{\Delta\lambda}$ by cirrus clouds is close to neutral and is 12-14% for Ci, 10-14% for Cc, 23-24% for Cs and 13-15% for all forms of clouds. For the spectral region $\lambda < 525$ nm the attenuation is somewhat greater: 19-27%. However, the error of determining $I_{\Delta\lambda}$ in this spectral interval perhaps is larger since it is determined from the small differences of large values.

It is evident from Table I.5, that the number of measurements in different regions of the spectrum is not equal. To exclude the inhomogeneity of data due to a different number of cases, average values of $P^o_{\Delta\lambda}$ and $\tau_{\Delta\lambda}$ were determined from the data of simultaneous measurements in all spectral intervals. This confirms the approximately neutral attenuation of direct radiation by high-level clouds.

It should be reminded (see section I) that values of $\tau_{\Delta\lambda}$ obtained by the actinometer are cut by about 50% and that the real $\tau_{\Delta\lambda}$ will be twice as big as the data of Table I.5. Correspondingly $P^o_{\Delta\lambda}$ will be less.

Table I.5. High-level clouds' mean transparency coefficient ($P^o_{\Delta\lambda}$) and optical thickness ($\tau_{\Delta\lambda}$). n - number of cases, v -variation coefficient.

		$P^o_{\Delta\lambda}$				$\tau_{\Delta\lambda}$			
Forms		Spectral Region,nm,				Spectral region, nm			
of clouds		$\lambda <$ 4000	$\lambda <$ 525	$\Delta\lambda =$ 380-710	$\lambda >$ 710	$\lambda <$ 4000	$\lambda <$ 525	$\Delta\lambda =$ 380-710	$\lambda >$ 710
Ci	med.	0.88	0.83	0.86	0.88	0.13	0.19	0.15	0.13
	n	106	49	77	85				
Cc	med.	0.90	0.81	0.88	0.86	0.11	0.21	0.13	0.15
	n	15	4	7	5				
Cs	med.	0.77	0.73	0.76	0.76	0.25	0.31	0.27	0.27
	n	11	7	11	11				
All forms	med.	0.87	0.82	0.85	0.86	0.14	0.20	0.16	0.15
	min.	0.55	0.50	0.56	0.53	0.01	0.02	0.01	0.01
	max	0.99	0.98	0.99	0.99	0.59	0.69	0.58	0.64
	V%	11	15	12	12	80	76	76	81
	n	146	68	108	114				
All forms (data of simultaneous measurements)	med.	0.84	0.82	0.84	0.84	0.17	0.20	0.17	0.17
	v%	12	15	12	13	72	77	68	78
	n	66	66	66	66				

b. Diffuse and global radiation. To evaluate the impact of cirrus clouds on Q and D, those cases with a solid cloud cover were chosen. Global radiation was determined in a minute and diffuse radiation in 0.5 hr.

Table I.6 lists mean (for all data of measurements), maximal and minimal values of global radiation in different regions of the spectrum.

Regular variations of diffuse radiation can be traced from the ratio for equal sun heights:

$$C_D = D/D_o$$

where D_o - diffuse radiation when the sky is clear and there is aerosol turbidity close to that which was observed on days with cirrus clouds.

Table I.6. Global solar radiation in different regions of the spectrum in conditions of the solid high cloud cover.

sun height-h°	14.2	22.4	32.6	42.6	52.3
		Integral radiation, Kw/m^2, $\lambda < 400$ nm			
Mean value	0.171	0.269	0.496	0.650	0.768
Maximum	0.192	0.355	0.613	0.804	0.873
Minimum	0.131	0.144	0.348	0.439	0.565
n	15	137	296	402	550
v%		19	14	12	9
		Ultraviolet radiation ($\lambda < 380$nm), W/m^2			
Mean	5.9	10.3	18.8	26.1	33.6
Maximum	6.3	12.8	23.8	32.3	38.8
Minimum	5.4	7.0	15.3	18.8	26.2
v%		14	16	12	7
		Photosynthetic active radiation ($\Delta\lambda = 380 - 710$ nm), Kw/m^2			
Mean	0.072	0.121	0.227	0.307	0.380
Maximum	0.080	0.162	0.268	0.370	0.440
Minimum	0.060	0.060	0.176	0.224	0.288
v%		26	11	11	7
		Near infrared radiation ($\lambda > 710$ nm), Kw/m^2			
Mean	0.093	0.138	0.250	0.317	0.354
Maximum	0.110	0.184	0.327	0.423	0.454
Minimum	0.066	0.067	0.154	0.188	0.239
v%		29	18	15	12

Note: n-number of cases V-variation coefficient

The results of calculations of C_D given in Table I.7 show an essential increase (with the exception of the uv region of the spectrum) of diffuse radiation in cirrus clouds which compensates to a large extent for the decrease of direct radiation. As a result, global radiation, as is evident from Figure I.9 varies relatively insignificantly. The character of the distribution of $C_Q = Q/Q_o$ for individual spectral intervals differs: the greatest C_Q range takes place in the case of near infrared radiation and the lowest in the case of ultraviolet radiation.

On average, high clouds attenuate by 4 - 6% the global radiation in the considered spectral regions.

Table 1.7. The effect of high clouds on the ration C_D.

Spectral region	Mean C_D	Maximum C_D	Minimum C_D	Number of cases	V%
int	1.35	3.51	0.93	96	38
uv	0.97	1.17	0.75	117	8
par	1.14	1.89	0.81	113	17
nir	1.62	3.65	1.01	110	34

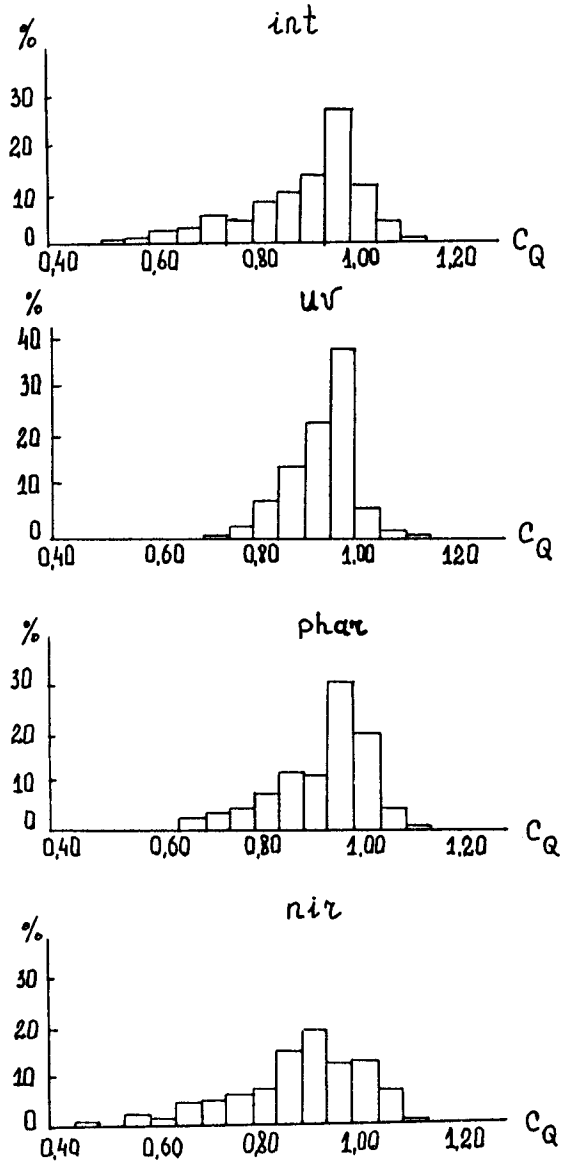

Fig. I. 9. Histograms of the ratios of global radiation for solid high cloud cover to cloudless sky - C_Q.

Part II. Calculations of radiation fluxes with cirrus clouds, based on the experimental data

1. Integral thermal radiation fluxes

Calculating these fluxes, we have applied the "continous approach" worked out and used earlier relating to water clouds (Feigelson, 1973).

The equations are:

for the semispherical upward flux:

$$F_{\uparrow}(Z) = B_s D(Z) + \int_0^z B(Z')dD(Z - Z') \tag{II.1.a}$$

for a downward flux:

$$F_{\downarrow}(Z) = -\int_z^{z^*} B(Z')dD(Z' - Z) \tag{II.1.b}$$

Here: $B_s = \sigma T_s^4$; $B(Z) = \sigma T^4(Z)$; $T(Z)$ - temperature at the altitude Z; T_s - the surface temperature.

In (II.1.a.):

$$D(Z) = \begin{cases} D_g(Z) & \text{for } Z < Z_b \\ D_g(Z)e^{-km_w(Z-Z_b)} & \text{for } Z \geq Z_b \end{cases} \tag{II.2.a}$$

In II.1.b:

$$D(Z) = \begin{cases} D_g(Z^* - Z) & Z \geq Z_t \\ D_g(Z^* - Z)e^{-km_w(Z_t-Z)} & Z < Z_t \end{cases} \tag{II.2.b}$$

where $D_g(Z)$ is the integral gaseous transmission function in the column $(O; Z)$; $m_w(Z - Z_b)$ - is the ice water content in a cloud layer $(Z_b; Z)$, accordingly, $m_w(Z_t - Z)$ - corresponds to the layer $(Z; Z_t)$; Z_b; Z_t - are cloud boundaries, and Z^* - the upper boundary of the atmosphere.

This approach helps to avoid errors of the usual type (given in the appendix). The errors result from the inapplicability of the superposition principle to the function D_g:

$$D_g(Z_1 + Z_2) \neq D_g(Z_1)D_g(Z_2) \tag{II.3}$$

Our approach allows also to calculate the fluxes inside the cloud and to evaluate errors for the second term of equations (I a, b in appendix).

The techniques, calculation results and assessment of errors are given in Feigelson (1988), Gorchakova and Feigelson (1989) and in the collection of papers "Radiative Properties of Cirrus Clouds" (1989, see Part I). Here results of calculations, based on the data of the ZSS experiment are presented. A few general remarks should be made in connection with the experimental data.

1. Using the data of aerological soundings of the temperature $T(Z)$ and moisture $q(Z)$ obtained at a distance of 80 km from the ZSS we have adjusted the profiles in such a way that $T(O)$ and $q(O)$ coincided with those directly measured in the place of the experiment.

2. In the case of the continuous approach we must know the height distribution of ice inside the cloud - $m_w(Z)$. We have supposed that $m_w(Z)$ is proportional to $\beta(Z)$ (see Part I, section 2) and $\mathrm{km}_w^*(Z_t - Z_b) = \tau_{\lambda_o}$ for $\lambda_o = 10.2\ \mu$m (see Part I, section 1).

Referring to two cases of measurements conducted on May 11 and 24, 1986, let us consider the errors of using the adopted equations (1.2.a, b) from the appendix when compared with the continuous approach. The results of the calculations are presented on Table II.1.

Table II.1. Values of radiative fluxes at the boundaries of the cloud ($F_\uparrow(z_t)$; $F_\downarrow(z_b)$) and at the boundaries of the atmosphere ($F_\uparrow(\infty)$; $F_\downarrow(0)$). Column 1-cloudless sky, columns 2-continuous approach, 3-calculation according to formulas (1.2.a, b, appedix).

Fluxes	May 11, 1986 $z_b = 7.9$ km, $z_t = 8.2$ km			May 24, 1986 $z_b = 6.0$ km, $z_t = 8.0$ km						
w/m²	$\tau = 0.18$			$\tau = 0.21$			$\tau = 0.53$		$\tau = 1.2$	
	(1)	(2)	(3)	(1)	(2)	(3)	(2)	(3)	(2)	(3)
$F_\uparrow(z_t)$	248	232	210	277	255	228	233	212	211	197
$F_\uparrow(\infty)$	220	205	166	235	216	176	196	169	176	163
$F_\downarrow(0)$	236	245	273	307	321	349	335	353	350	358
$F_\downarrow(z_b)$	70.3	86.0	104	132	158	191	184	210	211	229

Let us consider the error of calculating the clouds own radiation, using the second term in equations 1.a, b of the appeddix. Apparently the error is small for thin cloud layers. In the case of thick layers $B(z_t)$ must be replaced by B_1 while $B(z_b)$ by B_2 expressed by the ratios:

$$B_1 = -\frac{\int_{z_b}^{z_t} B(z')dD[z_t - z']}{1 - D[z_t - z_b]}; \qquad B_2 = \frac{\int_{z_b}^{z_t} B(z')dD[z' - z_b]}{1 - D[z_t - z_b]} \tag{II.4}$$

These equations represent the weighted mean values of $B(z)$ in limits $(z_b; z_t)$.

Table II.2 Values B_1 and B_2; Column (1)-max $W(z)$-near the upper boundary; (2)-in the center of the cloud; (3)-near the lower boundary.

$B_1 w/m^2$			$B(z_t) w/m^2$	$B_2 w/m^2$			$B(z_b) w/m^2$
(1)	(2)	(3)		(1)	(2)	(3)	
193	200	222	190	214	222	235	238

In Table II.2 for May 24, 1986, values B_1 and B_2 are given depending on the position of max $W(z)$ $(W(z) = dm_w(z)/dz)$.

Thus, the error in using formulas (1.a,b) appendix can be large if the thick clouds radiation is referred to their own boundaries.

Let us assess the error of the same equations if we neglect gas absorption. Assuming that fluxes calculated by the continuous method are exact (at least their error is the same as in the cloudless case), let us substitute their values into (1.a, b) and then determine the emissivity ε and $D_g(z_t - z_b) = \frac{1-\varepsilon}{e^{-1.66\tau}}$. The values of D_g obtained are listed in Table II.3.

Table II.3. True values of D_g; May 24, 1986

τ	$D_{g,\uparrow}(\Delta m)$	$D_{g,\downarrow}(\Delta m)$
0.21	0.72	0.71
0.53	0.73	0.70
1.2	0.76	0.76

We see that the true values of $D_g(z_t - z_b)$ are far enough from unity. However, it is not clear how an *a priori* method of determining these true values can be evolved, as well as $D_g[z - z_t]$, $D_g[z_b - z]$ in eqs. 2.a, b appendix.

Therefore, we recommend the continuous approach for calculating integral thermal radiation fluxes. The advantages of this method are obvious: a single algorithm for calculations for cases when the sky is cloudy and when it is clear.

The values of fluxes as compared with the case of the clear sky are given in Table II.1 for 1986 and in Table II.4, for 1987. Table II.5 gives the radiative cooling of the atmospheric layers. This table shows that the atmosphere become warmer during the cloudy sky, as compared with the case of the clear sky. The same is true for the subcloud layer. The above-cloud layer is cooling. The cloud, depending on its height, thickness, temperature and moisture distribution, can become warmer or colder than the corresponding layer of the cloudless atmosphere.

Table II.4. Integral radiation fluxes, for the year 1987.

Date	May 19		May 20		May 22	
Fluxes W/M^2	clear sky	cloudy sky $z_b = 8.4$ $z_t = 9.4$ $\tau = 0.33$	clear sky	cloudy sky $z_b = 8.5$ $z_t = 10$ $\tau = 0.17$	clear sky	cloudy sky $z_b = 7.5$ $z_t = 8.1$ $\tau = 0.46$
$F_\uparrow(z_t)$	240	206	241	218	254	217
$F_\uparrow(\infty)$	216	186	223	203	208	179
$F_\downarrow(z_b)$	93	124	95	111	117	156
$F_\downarrow(0)$	309	321	344	350	372	383

Table II.5. Radiative cooling in W/m^2 of different layers: 1 - the whole atmosphere; 2 - the above cloud layer; 3 - the subcloud; 4 - the cloud layer. Positive sign is cooling.

Date 1987	May 19		May 20		May 22	
Layers	clear sky	cloudy sky $\tau = 0.33$	clear sky	cloudy sky $\tau = 0.17$	clear sky	cloudy sky $\tau = 0.46$
1	121	104	123	110	131	113
2	52	56	51	54	58	66
3	68	49	70	60	71	43
4	1.9	-1.9	1.8	-4.7	2.3	4.2

Let us discuss in conclusion the problem of taking into account the reflection of flux $F_\uparrow(z_b)$ by the cloud within the framework of the same parametrization. For the sake of simplicity we can limit ourselves to a slight decrease of the coefficient K in eq. II.2b. However, the possibility of taking into account actual variations of $F_\uparrow(z_b)$ is then lost.

The second possibility is to calculate the flux $F_\downarrow(z_b)$ from eq. (II.1.b) to which the component $AF_\uparrow(z_b)$ is added.

The albedo A can be determined from the data given by Liou and Wittman (1979) wich represent, however, a particular case: $z_b = 4.6$, the particles are cylindrical with $1 = 200$ μm, $r = 30$ μm, and the number of particles is 0.05^{-3} cm. In Feigelson (1988) a more general, although approximate approach has been presented, based on the solution of radiative transfer equation in case of multiple scattering. The formula obtained makes it possible to change the flux $F_\uparrow(z_b)$ and also the optical parameters of the cloud:

$$F_\downarrow(Z_b) = \varepsilon \frac{\omega F_\uparrow(z_b)\Gamma_2 + (1-\omega)B(z_b)}{1 - \omega\Gamma_1\varepsilon} \tag{II.5}$$

where $\Gamma_1 = \int_o^1 \gamma(\phi) d\cos\phi$ and $\Gamma_2 = \int_{-1}^o \gamma(\phi) d\cos\phi$; $\gamma(\phi)$ is the scattering function; ϕ - the scattering angle; ω - the single scattering albedo; ε - the emmissivity.

2. Optical models used in the calculation of solar radiation

To calculate the solar radiation fluxes in the presence of cirrus clouds we need to know the following optical parameters of the clouds: the asymmetry factor of the phase function - g (the δ - Eddington approximation is used for flux calculations), the single scattering albedo - ω and the optical thickness - τ of the clouds which we get experimentally (see Part I, secion 1).

In Volkovitsky *et al.* (1984) the technique for determining g and ω for hexagonal prisms with a gamma-distribution of paticles size was described and some calculations were made. In our paper, using the above technique, more detailed calculations were carried out for hexagonal ice prisms large as compared with the wavelength and having chaotic orientation in space. A gamma-

distribution of particle lenghts - l was used:

$$f(l)dl = Nl^{\mu} \exp(-\mu l/l_m)dl \tag{II.6}$$

where N is the normalization constant, l_m - the model length of the prism, and $\mu = 6$ - the gamma-distribution parameter. We considered the fraction of large ice particles with $50 < l_m < 10^3$ μm and the shape factor varied within $0.5 < c = l/d < 6$. Here d is the diameter. The refractive index of ice was taken from Irvine and Pollack (1978).

a. The asymmetry factor. Phase functions $P(\theta)$ of large ice prisms were calculated in the geometrical optics approximation with due account for diffraction. A typical phase function is given in Figure II.1. When $\theta < \theta_d$, where $\theta_d \approx 10^{\circ}$ is the diffraction angle, the form of the phase function depends on the size and shape factor of hexagonal prisms. At the same time in the range of sizes 20 μm $< l_m <$ 400 μm, $1 < c < 6$ with $\theta < \theta_d$, the difference of the values of phase function for prisms and model ice spheres is less than 30% to 40%. Thus, the model for spherical particles having the same surface area as hexagonal prisms describes with a rather satisfactory accuracy

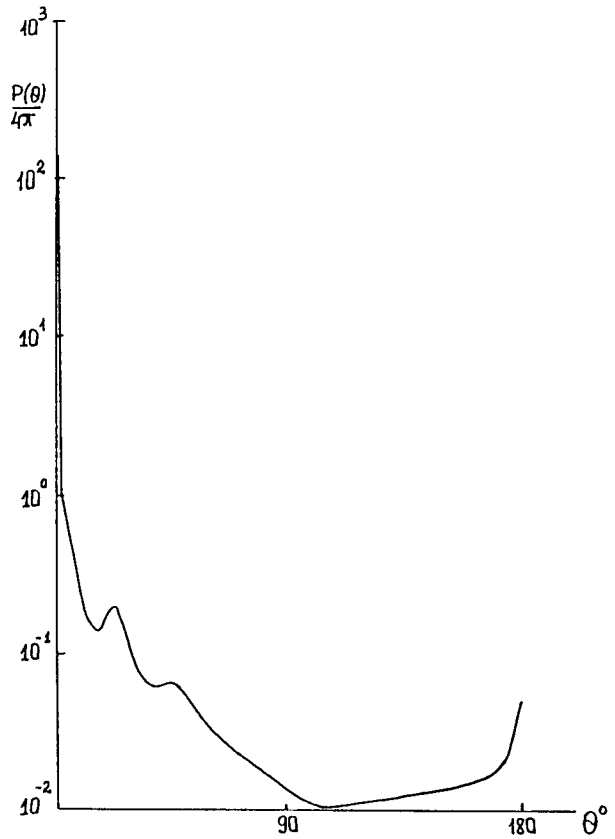

Fig. II. 1. Phase function of visible radiation $\lambda = 0.63$ μm by a system of hexagonal prisms with gamma-distribution in lenghts ($1_m = 200$, $c = 4$).

the scattering by a system of hexagonal prisms for small angles $\theta < \theta_d$. When $\theta > \theta_d$ no model for spherical particles represent scattering by prisms since the specific features of such scattering are mainly determined by the particle's nonspherical shape.

Values of g were determined through the numerical integration of the obtained phase functions. Since for particles with size considerably exceeding the wavelength scattered flux with $0 \leq \theta \leq \theta_d$ is roughly equal to the scattered flux with $\theta_d < \theta \leq \pi$, the expression for g can be roughly written in the form

$$g \approx \frac{\int_0^{\theta_d} P(\theta) \cos\theta \sin\theta d\theta}{2\int_0^{\theta_d} P(\theta) \sin\theta d\theta} + \frac{\int_{\theta_d}^{\pi} P(\theta) \cos\theta \sin\theta d\theta}{2\int_{\theta_d}^{\pi} P(\theta) \sin\theta d\theta} \tag{II.7}$$

With the increase of the size of the prisms the first term slightly increases, tending to its limiting value of 0.5. The second term practically does not depend on the size. Thus, the asymmetry factor, with the increase of the size of the prisms of fixed shape, tends to a certain limiting value. These limit values were detected earlier for large spherical particles (Van de Hulst, 1957) and they are only function of the complex refractive index for the wave length under consideration. The value $g = 0.87$ was obtained for water spheres irrespective of dimensions when $\lambda = 0.6$ μm. The result of the integration of the phase function represented in Figure II.1 is $g = 0.74$ for ice hexagonal prisms with $c = 4$. The main contribution to the change of g (from spheres to hexagonal prisms) is made by the scattering angle range from 10° to 50° of the phase function.

b. Single scattering albedo. Calculations of the single scattering albedo - ω for individual hexagonal prisms and for systems of hexagonal prisms with arbitrary values of the shape factor c and chaotic orientation in space were performed. The size and the shape factor of crystals varied within the ranges $10^2 < l_m < 10^4$ μm, and $0.5 < c < 6$. The calculation procedure used in the approximation of geometric optics made it possible to take into account the contribution to the absorption by multiple refraction and reflection events on lateral facets of the prism, as well as single reflection and refraction on butt-ends of the prism.

The results of the calculations we have carried out show that when $\lambda < 1.2$ μm for the considered range of values of l_m the value ω is essentially different from 1 only when $l_m > 10^3$ μm. With the increase of λ the value ω greatly depends on the size and can assume the values ranging from 0.6 to 0.9. As an effective size a_{ef} of hexagonal prisms in describing the single scattering albedo let us use the ratio of the volume of crystals to the area of the geometrical shadow. This effective size was first proposed in Van de Hulst (1957) for describing the attenuation by systems of spherical particles.

The comparison of the calculations of ω for systems of hexagonal prisms and for circular cylinders of finite length (Liou, 1973) with calculations for large ice spheres with effective size a_{ef} carried out according to the Mie theory shows satisfactory agreement. In the range of wavelengths of the incident radiation $\lambda = 0.63 - 2.5$ μm it is logical to use approximate expressions for ω for individual ice particles:

$$\omega = \begin{cases} 1 - 0.5 f(n)\gamma a_{ef} & \gamma a_{ef} < 0.1 \\ 0.5 + 0.5\exp(-f^k(n)\gamma a_{ef}) & \begin{cases} k=1 & \gamma a_{ef} < 0.5 \\ k=2 & 0.5 < \gamma a_{ef} < 2.5 \end{cases} \\ 0.5 + 0.5\omega_o & \gamma a_{ef} > 5 \end{cases} \quad \text{(II.8)}$$

For systems of particles with gamma-distribution of sizes:

$$\omega = 0.5 + 0.5\left[1 + \frac{f^2(n) a_{ef}\gamma}{(\mu+3)}\right]^{-(\mu+3)}, \quad a_{ef}\gamma < 3 \quad \text{(II.9)}$$

Here μ is gamma-distribution parameter, ω_o - the fraction share of radiation reflected by a sphere (Kerker, 1969), $a_{ef} = 2l_o(1 + \frac{4}{\sqrt{3}}c)^{-1}$; l_o - length of the prism in the case of individual particles, or modal length for systems of particles; $f(n) = n^2\{1 - [(n^2-1)/n^2]^{3/2}\}$; $\gamma = (4\pi k/\lambda)$, k - imaginary part of refractive index.

The application of these expressions for calculating ω of hexagonal prisms leads to the absolute error not higher than 0.05 in the entire range of considered dimensions of prisms.

3. Calculation of fluxes of solar radiation. Table II.6 gives four models of the optical characteristics of the cloud layer which are used in calculations.

Table II.6. Optical Characteristics of Particles of Different Shapes. The value of g corresponds to the spectral interval $0.3 < \lambda < 4$ μm; $\omega = \omega_1$ for $0.3 < \lambda < 1.2$ μm, ω_2 for $1.2 < \lambda < 2.5$ μm; ω_3 for $\lambda > 2.5$ μm.

Model	Shape	$c = 1/d$	g	ω_1	ω_2	ω_3
I	Spherical	1	0.87	1	0.9	0.5
II	Spherical	1	0.87	1	0.6	0.5
III	Hexagonal	4	0.74	1	0.9	0.5
IV	Prisms	4	0.74	1	0.6	0.5

Due to our investigation of the optical parameters the value of g for large particles $a_{ef} > 10$ μm does not depend on the size but depends on the factor of the particle shape $c = 1/d$. So, models I and II were constructed for spherical particles with $c = 1$ and model III and IV - for hexagonal prisms with $c = 4$. We used one value of g for all the solar spectrum. The increase of g with the considerable absorption of ice when $\lambda > 2.5$ μm was ignored due to the weak influence of g on the radiative transfer in this case.

Single scattering albedo ω_2 in the wave length interval $1.2 \leq \lambda \leq 2.5$ μm has the strong dependence on the particle sizes. We have made models II and IV with $\omega_2 = 0.6$, as limited value for very large particles $a_{ef} > 10^2$ μm. The value $\omega_2 = 0.9$ is more realistic for particles in cirrus clouds. With the help of these four models we wanted to determine the sensitivity of solar fluxes to g and ω_2.

Spectral optical thicknesses of cirrus of clouds τ_λ were determined from measurements. We used half hour average values of $\bar{\tau}$ for $\lambda = 10.2$ μm, which were free from the multiple scattering effects (see Part I, section 1).

The optical characteristics of the extracloud aerosol atmosphere were determined in the course of the experiment or varied within wide limits in accordance with the aerosol models described in Tarasova and Feigelson (1981), and "rural" and "background stratospheric" models (WCP-55, 1983). The values of the aerosol optical thicknesses τ_a, λ were determined from measurements of direct solar radiation ($0.38 < \lambda < 0.71$ μm) according to the technique given by Abakumova *et al.* (1989), the values of water vapour amount m_v were taken from aerological soundings.

To calculate the integral fluxes of solar radiation, use was made of three-layer model of the cloud-aerosol atmosphere. In the lower, sub-cloud layer we took into account molecular scattering, absorption, scattering by aerosol and absorption by water vapour; in the cloud layer - scattering and absorption by ice crystals, and in the upper layer molecular scattering and scattering and absorption by aerosol. Calculations were carried out using the δ - Eddington's method (Joseph *et al.*, 1976) in 12 spectral intervals from $\lambda = 0.3$ μm to $\lambda = 4$ μm, including six water vapour bands. For water vapour bands use was made of the expansion of the transmission function of the water vapour into a series of five exponentials, given by Liou, and Sasamori (1975). We calculated the integral global radiation $Q(0.3 < \lambda < 4$ μm) and the photosynthetically active global radiation ($0.38 \leq \lambda \leq 0.71$ μm) near the surface. The system's albedo - A (atmosphere - underlying surface) was also calculated for the same wave length intervals. The spectrum of the solar constant from WCP-149, 1986 was used.

The albedo of the surface was given within the limits $A_s = 0.1 - 0.2$ which corresponds to the albedo of grass and coniferous forests from Kondratyev (1960).

To compare calculated and measured fluxes we choose observation periods which are characterized by almost solid cirrus clouds with the absence of other forms of clouds in the sky.

The results of measurements and calculations are summarized in Tables II.7-II.9. The interval of values Q^{calc} and A corresponds to the stated ranges of the change of the cloud and aerosol optical parameters.

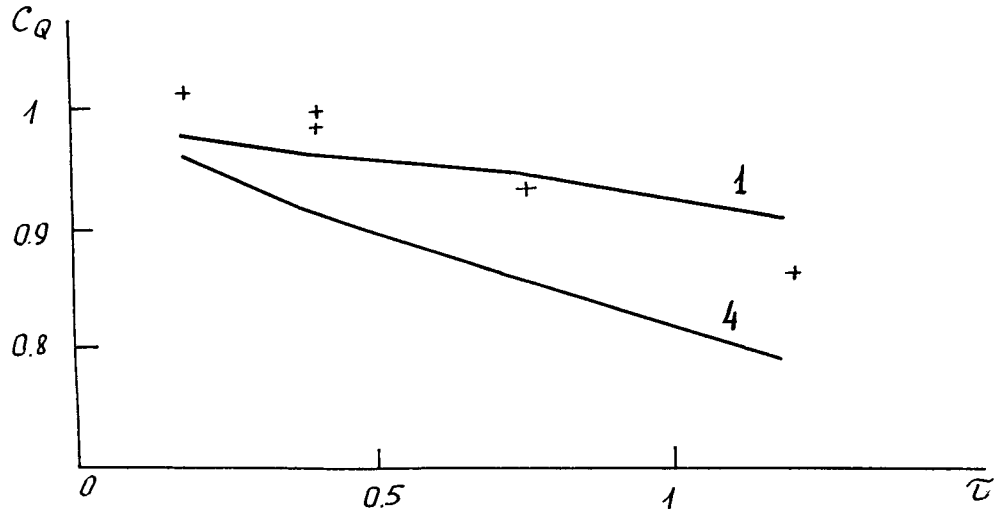

Fig. II. 2. C_Q value for observation periods indicated in Tables II.7 - II.9. This value is calculated for two models giving the minimum and maximum values: 1 and 4. The crosses are the experimental data.

Values of Q^{calc} and Q^{meas} agree within the limits of the errors of calculations and measurements which are of the order of 10%.

To assess quantitatively the effect of Ci on the global radiation flux we have calculated the ratio $C_Q = Q_{cloud}/Q_{clear}$ of fluxes during cloudy and clear sky. This ratio is given in Tables II.7-II.9 and in Figure II.2.

The values C_Q are determined by the optical parameters of the cloud τ, g, ω_2. We use the linear approximation:

$$C_Q = 1 - 0.19\tau' \tag{II.10}$$

where $\tau' = (1 - g^2\omega_2)\tau/\mu_o$ with good accuracy. The error of calculating C_Q by the formula II.10 is less than 1% when $\tau < 1$ and less than 2% when $\tau > 1$. It is evident from Tables II.7-II.9 that the calculated values of C_Q are in good agreement with measured values, with the exception of thin clouds $0.1 < \tau < 0.2$ when $C_Q^{meas} > 1$. This effect is possibly due to the greatly broken field of thin cirrus clouds. In this case the contribution of direct solar radiation to global radiation can be greater than in the model of a homogenous cloud layer used in the calculations.

Table II.7. Calculated (*calc*) and measured (*meas*) integral fluxes of global radiation near the surface - Q, with the Ci (cloud) and without the Ci (clear) for 1986. The table lists also ratios - $C_Q = Q_{cloud}/Q_{clear}$ and changes of system albedo A by the clouds - $C_A = A_{cloud}/A_{clear}$. Θ_o - solar zenith angle; τ_a, λ_o - aerosol optical thickness at $\lambda_o = 0.55$ μm.

	11.V.86			24.V.86		
$\mu_o = \cos\Theta_o$	0.771	0.79	0.729	0.807	0.817	0.763
$\overline{\tau}$	0.18	0.17	0.41	0.41	0.75	1.2
τ_a, λ_o	0.15-0.25	0.3-0.5	0.3-0.5	0.3-0.5	0.3-0.5	0.3-0.5
$m_v, g/cm^2$	0.5	1.8	1.8	1.8	1.8	1.8
Q_{cloud}^{calc}	850-784	823-718	745-611	831-701	827-666	738-554
Q_{cloud}^{meas}	862	816	719	805	765	660
Q_{clear}^{calc}	860-799	837-745	762-673	858-765	870-777	804-713
Q_{clear}^{meas}	839	797	723	817	827	767
C_Q^{calc}	0.99-0.98	0.98-0.96	0.96-0.91	0.97-0.92	0.95-0.86	0.91-0.78
C_Q^{meas}	1.02	1.02	1.00	0.99	0.94	0.86
C_A^{calc}	1.12-1.01	1.09-1.00	1.23-1.02	1.23-1.01	1.38-1.03	1.6-1.07

Table II.8. The same as in Table II.7 but for fluxes in the wavelenghts of photosynthetically active radiation ($0.38 \leq \lambda \leq 0.71$ μm).

Date	11.V.86			24.V.86		
μ_o	0.771	0.79	0.729	0.807	0.817	0.763
Q^{calc}_{cloud}	399-365	401-346	361-300	408-343	409-333	368-285
Q^{meas}_{cloud}	381	412	364	408	399	344
Q^{calc}_{clear}	402-375	403-354	367-320	414-364	420-370	388-339
Q^{meas}_{clear}	387	397	359	408	415	381
C^{calc}_{Q}	0.99-0.97	1.00-0.98	0.98-0.94	0.99-0.94	0.97-0.9	0.95-0.84
C^{meas}_{Q}	0.99	1.04	1.01	1.00	0.95	0.94
C^{calc}_{A}	1.09-1.02	1.06-1.02	1.17-1.05	1.17-1.04	1.29-1.08	1.45-1.13

Table II.9. The same as in Table II.7-8, but for 1987.

	Integral radiation				Photosynthetically active radiation			
	19.V.87		20.V.87	20.V.87	19.V.87		20.V.87	22.V.87
$\mu_o = \cos\Theta_o$	0.80	0.51	0.76	0.81	0.80	0.51	0.76	0.81
$\overline{\tau}$	0.32	0.33	0.17	0.46	0.32	0.33	0.17	0.46
τ_a, λ_o	0.2-0.3	0.2-0.3	0.45-0.60	0.45-0.60	0.2-0.3	0.2-0.3	0.45-0.60	0.45-0.60
$m_v, g/cm^2$	1.3	1.3	1.9	2.8	1.3	1.3	1.9	2.8
Q^{calc}_{cloud}	845-756	494-420	758-655	807-672	409-367	239-205	372-314	402-332
Q^{meas}_{clear}	750	391	719	721	366	189	350	358
Q^{calc}_{cloud}	862-809	513-469	767-681	829-741	414-383	245-220	374-323	409-355
Q^{meas}_{clear}	850	475	779	865	421	224	380	425
C^{calc}_{Q}	0.98-0.93	0.96-0.9	0.99-0.96	0.97-0.91	0.99-0.96	0.98-0.93	0.99-0.97	0.98-0.94
C^{meas}_{Q}	0.88	0.82	0.92	0.83	0.87	0.84	0.92	0.84
C^{calc}_{A}	1.21-1.00	1.27-1.04	1.10-1.00	1.23-1.02	1.15-1.03	1.19-1.06	1.06-1.02	1.16-1.04

The influence of the microstructure of the cloud and albedo of the underlying surface A_S on the ratio of atmosphere-surface albedo with cloud and without $C_A = A_{cloud}/A_{clear}$ is presented in the Figure II.3 for two extreme cases (models II and III). A simple approximation formula for determining C_A was obtained:

$$C_A = \frac{1 + k(g)\tau}{1 + A_S/0.14} + \frac{A_S C_Q^2}{A_S + 0.14} \qquad \text{(II.11)}$$

where $k(g) = 0.8$ when $g = 0.7$ and $k(g) = 0.4$ when $g = 0.9$. The error of using equation II.11 is smaller than 3% when $\tau < 1$ and less than 5% when $\tau > 1$.

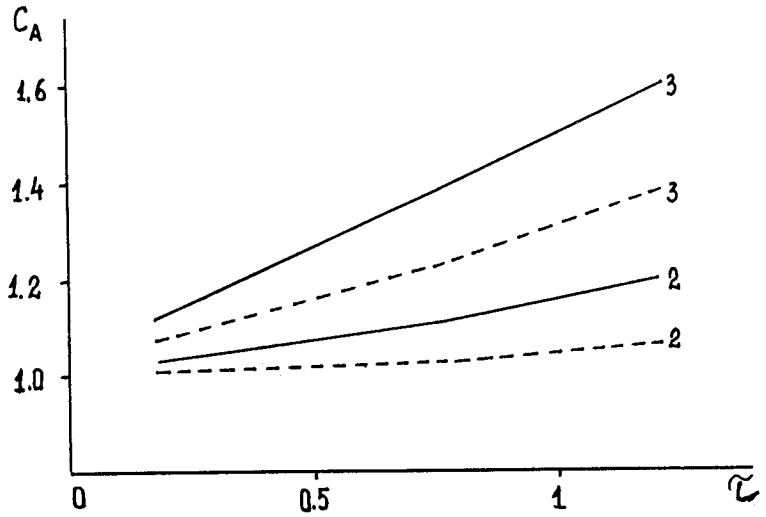

Fig. II. 3. Value C_A with different albedos of the surface (solid curves - $A_s = 0.1$, dashed curves $A_s = 0.2$) for two models giving the maximum and minimum values: 2 and 3.

4. Radiation balances. The radiation balance at the upper boundary of the atmosphere $F(\infty)$ in the case of cirrus clouds and for the cloudless atmosphere was obtained from the formula

$$F(\infty) = I_o \mu_o (1 - A) - F_\uparrow(\infty). \tag{II.12}$$

Where I_o - solar constant, μ_o - cosine of the Sun's zenith angle, $F_\uparrow(\infty)$ - outgoing thermal radiation flux calculated (the same as the albedo - A) from the data of the experiment. High clouds reduce $F_\uparrow(\infty)$, and increase A. Depending on the ratio of these opposite trends the value of the change of the radiation balance produced by the cloud:

$$\Delta F(\infty) = F_{cloud}(\infty) - F_{clear}(\infty) \tag{II.13}$$

can have a different sign.

We have also calculated the change of the radiation balance of the underlying surface in the presense of Ci clouds compared with the cloudless atmosphere

$$\Delta F(O) = F_{cloud}(O) - F_{clear}(O) \tag{II.14}$$

where $F(O) = F_\downarrow(O) - F_\uparrow(O) + I_o \mu_o t(1 - A_s)$; $F_\uparrow(O)$ - thermal radiation of the surface; $F_\downarrow(O)$ - thermal radiation of the atmosphere; t - transmission of the atmosphere for solar radiation. Finally we calculated the change of the radiation balance or the influx of the atmosphere:

$$\Delta F_a = \Delta F(\infty) - \Delta F(O) \tag{II.15}$$

The results of calculations are given in table II.10.

For the sake of comparison appropriate variations of balances for thermal radiation are also listed in this table:

$$F^{therm}(\infty) = -F_{\uparrow}(\infty)$$

$$F^{therm}(O) = F_{\downarrow}(O) - F_{\uparrow}(O)$$

$$F_a^{therm} = F^{therm}(\infty) - F^{therm}(O) \qquad \text{(II.16)}$$

As it is evident from Table II.10 when clouds have optical thickness $\tau \geq 0.3$ (with due account of the non-spherical character of particles), we obtained that despite the weakening of the long-wave cooling by clouds, the radiative heating of the system decreases due to the stronger reflection of solar radiation and $\Delta F(\infty) = (-3) - (-18) \mathrm{W/m^2}$. For models of spherical particles an increase of the balance $F(\infty)$ by the value 14-25 $\mathrm{W/m^2}$ was obtained.

The change of the atmosphere influx are always positive and almost do not depend on the values of A_s assumed in the calculations. The influx itself can be both positive or negative. Close values ΔF_a for models I and III (the same as for models II and IV) mean that the main influence on the influx is exerted not by the shape, but by the absorption of particles, i.e., by the parameter ω_2 depending on the ice complex refractive index and the size of particles.

Table II.10. Variations of the radiation balance of the upper boundary of the atmosphere $\Delta F(\infty)$, the surface $\Delta F(O)$ and the influx to the atmosphere ΔF_a in the event of cirrus clouds as compared with the cloudless atmosphere; corresponding variations fo the long-wave radiation balance (thermal) $\mathrm{W/m^2}$.

Date	$\bar{\tau}$	m_v, $\mathrm{g/cm^2}$	Optical cloud model	$\Delta F(\infty)$		$\Delta F(O)$		ΔF_a		$\Delta F(\infty)$	$\Delta F(O)$	ΔF_a
				$A_s = 0.1$	$A_s = 0.2$	$A_s = 0.1$	$A_s = 0.2$	$A_s = 0.1$	$A_s - 0.2$		thermal	
19.5.87.	0.33	1.3	I	15	18	-5	-3	20	21			
			II	18	23	-16	-13	34	36			
			III	-9	-4	-24	-19	15	15	30	12	18
			IV	-4	-3	-32	-25	28	28			
20.5.87	0.17	1.9	I	14	16	-2	-2	16	18			
			II	16	19	-7	-7	23	26			
			III	1	5	-13	-10	14	15	20	6	14
			IV	4	8	-18	-15	22	23			
22.5.87	0.46	2.8	I	14	19	-11	-6	25	25			
			II	18	25	-24	-21	42	46			
			III	-18	-9	-38	-29	20	20	29	11	18
			IV	-11	-1	-50	-42	39	41			

Variations of the radiation balance of the surface have a negative sign, i.e., in the daytime the surface becomes colder due to the decrease of the solar radiation despite the decrease of the cooling by thermal radiation. (See $\Delta F^{therm}(O)$).

The calculations have shown the considerable sensitivity of the radiation regime, in the event

of cirrus clouds, to the chosen optical model of the cloud. To specify the obtained estimates it is necessary to have detailed experimental data on the distribution of cloud particles as far as their size, shape and optical characteristics are concerned.

Conclusion

The studies refer to the specific middle latitude region, day time conditions and spring-summer season.

The month of May was chosen for the experiment because of the many year's observations of clouds carried out at the Moscow University Meteorological Station in Moscow.

The state of the sky at the time of the experiment for two years in May, was the following: from the overall number of cases of cloudiness 40% corresponded to *Ci*. In 37% of these cases other clouds were not observed. These estimates agree quite well with the data of Table 1 from Hahn *et al.* (1984) where the global distribution of *Ci* during different seasons over dry land and the ocean is shown based on ground visual observations.

Table 1.

	Winter	Spring	Summer	Autumn
1	46/30	47/32	41/31	42/31
2	45/9	41/10	33/9	38/9

Line 1 in the table shows the percentage of *Ci* from all clouds under observation. Line 2 shows the percentage of the absence of other types of clouds while in presence of *Ci*. The numerator refers to observations over dry land, the denominator to observations over the ocean.

It is seen that even in case of the global averaging, spring is a good period for observations.

According to aircraft observations in the Moscow Region (Baranov, 1964) the formation of *Ci*, in 80% of cases is linked with atmospheric fronts - more with warm fronts than with cold fronts and more in a warm season than in a cold one. Cirrus clouds emerge at a distance of about 800 km before the front line. They are thin but are visible from the surface. With the approach to the front line the clouds become thicker and most frequently lie over the lower clouds.

The weather in May 1986 was colder than usual. The formation of *Ci* was mainly caused by cold fronts. These fronts were low and mostly occluded, that is why the upper clouds had no good development. In May 1987 the warm anticyclonic weather prevailed. The front were stationary or occluded. The warm weather and weak pressure gradient promotes the formation of *Cu* and *Cb* and thanks to that cirrus clouds were higher and dense.

The question arises: what do we study in the ground-based experiment?

We study thin cirrus clouds more frequently than thick clouds (geometrically and optically). This is confirmed by the results of the Part I. It is reasonable to study thin clouds for several reasons.

1. The radiative effect of the thin clouds is not a small one.

2. Thin clouds over the underlying surface with a small albedo (0.1-0.2) in spring in the region of the experiment have a greater effect on the albedo of the system than dense clouds which lie over a surface with a big albedo, for instance, by clouds lying below.

3. The variable greenhouse effect is created precisely by thin clouds. When $\tau > 2$ the cloud becomes black and, correspondingly, radiation from the boundaries is determined only by the temperature.

4. Thin clouds are poorly detected from satellites.

The purpose of the study was to determine the effect of cirrus clouds on integral (by the spectrum of wavelengths and by the directions) fluxes of solar and thermal radiation in order to introduce the results into the numerical models of the theory of the climate and the weather forecast.

We consider the following results of our study to be the most important:

1. The statistics of the heights and thicknesses of Ci clouds, of their optical parameters (spectral transparency of solar radiation, scattering coefficients in visual range, emissivity) and of the diffuse and global solar radiation at the Earth's surface.

2. Determination of the actual optical thickness of Ci clouds and the influences of scattered solar light on it.

3. Elaboration of models of optical parameters. Using them together with the measured optical thicknesses to calculate the radiative fluxes and to evaluate the influence of Ci clouds on them. Comparison of the calculated and the measured solar fluxes coming to the Earth's surface.

4. Elaboration of a new more precise "continuous" method for calculation thermal radiation fluxes. Evaluation of the influence of Ci clouds on fluxes divergences of integral thermal radiation.

The experiment was continued in 1989. The results of the 1989-1990 years work will be presented latter.

Appendix

Equations usually used for calculating the thermal radiation fluxes in the presence of clouds.

$$F_{\uparrow}(Z_t) = (1-\varepsilon)F_{\uparrow}(Z_b) + \varepsilon B(Z_t) \tag{1a}$$

$$F_{\downarrow}(Z_b) = (1-\varepsilon)F_{\downarrow}(Z_t) + \varepsilon B(Z_b) \tag{1b}$$

$$F_{\uparrow}(Z) = F_{\uparrow}(Z_t)Dg(Z-Z_t) + \int_{Z_t}^{z} B(Z')dDg(Z-Z')$$

$$\text{by } Z \geq Z_t \tag{2a}$$

$$F_{\downarrow}(Z) = F_{\downarrow}(Z_b)Dg(Z_b - Z) - \int_Z^{Z_b} B(Z')dDg(Z' - Z)$$

$$\text{by } Z \leq Z_b \tag{2b}$$

$$\varepsilon = 1 - e^{-km_w^*} = 1 - e^{-1.66\tau}$$

m_w^* - whole water content into the cloud.

REFERENCES TO PART I

Anikin, P. P., A. I. Chavro, and A. Kh. Shukurov, 1981. A complex optical installation for studying the spectral transmission of the atmosphere on oblique and horizontal routes in the ultraviolet, visible and infrared spectral ranges (0.3-25 μm). In: The physical aspects of the Remote Sensing of the Ocean-Atmosphere System, Moscow, Nauka Publishers. (In Russian).

Platt, C. M. R., J. C. Scott and A. C. Dilley, 1987. Remote Sounding of High Clouds: Part VI: Optical Properties of Midlatitude and Tropical Cirrus, *J. Atmos. Sci.*, vol. **44**, No. 4, pp. 729-747.

Zhuravlyova, V. A., S. F. Kalachinsky and O. K. Kostko, 1983. Joint IR-radiometric and lidar studies of radiation characteristics of cirrus clouds. Izvestiya Akademii Nauk SSSR, Fizika Atmosfery i Okeana (Physics of the Atmosphere and Ocean), vol. **19**, pp. 1167-1171.

Zhuravlyova, V. A., O. K. Kostko, 1986. Lidar-radiometric method of determination of the ice content of cirrus clouds. Ibid. v. **22**, pp. 44-52.

Zuyev, V. Ye., G. M. Krekov, M. Krekova and I. E. Naats, 1976. Theoretical Aspects of the Laser Sounding of Clouds. In: Problems of the Laser Sounding of the Atmosphere. Novosibirsk, Nauka Publishers. (In Russian).

REFERENCES TO PART II AND TO CONCLUSION

Abakumova, G. N., I. N. Plakhina and T. A. Tarasova, 1989. The estimate of the aerosol optical thickness of the atmosphere from the data of ground based and ship-based actinometry (comparison of various techniques). Meteorologiya i Gidrologiya. No. 10, pp. 45-54.

Baranov, A. A. 1964. Frontal Clouds and Conditions of Flights in Them. Leningrad. Gidrometeoizdat Publishing House, pp. 240. (In Russian).

Feigelson, E. M., 1973. Radiant heat transfer in a cloudy atmosphere. Translated from Russian. Published for NOAA by IPST, pp. 191.

Feigelson, E. M., 1988. Fluxes of infrared thermal radiation in cirrus clouds. Izvestiya Akademii Nauk SSSR. FAO series, Vol. **24**, No. 8, pp. 586-593.

Gorchakova, I. A. and E. M. Feigelson, 1989. Estimates of the errors of semi-black approximation. Izvestiya Akademii Nauk SSSR. FAO series, vol. **25**, No. 1.

Hahn, C. J., S. G. Warren, J. London, R. M. Chervin, R. Yenne, 1984. Atlas of Simultaneous Occurrence of Different Cloud Types over Land. NCAR Techn. note T 241 STR, Boulder company, pp. 21 + 180 maps.

Van de Hulst, 1957. Light Scattering by Small Particles. Wiley, New York, pp. 536.

Irwine, W. W. and J. B. Pollack, 1968. Infrared optical properties of water and ice spheres. Icarus, vol. **8**, No. 4, pp. 321-360.

Joseph, J. H., W. J. Wiscombe and J. A. Weinman, 1976. The Delta-Eddington approximation for radiative flux transfer *J. Atm. Sc.*, vol. **33**, No. 12, pp. 2452-2459.

Kerker, M., 1969. The Scattering of Light and Other Electromagnetic Radiation. New York-London. Academic Press, pp. 645.

Kondratyev, K. Ya., 1960. The spectral albedo of natural underlying surfaces. *Meteorologiya i Gidrologiya,* No. **5** pp. 46-53.

Liou, K. N., 1973. Transfer of solar irradiance through cirrus cloud layers. *J. Geophys. Res.*, vol. **78**, No. 9, pp. 1409-1418.

Liou, K. N., T. Sasamory, 1979. On the transfer of solar radiation in aerosol atmosphere. *J. Atm. Sci.*, Vol. **32**, No. 11, pp. 1166-1177.

Liou, K. N., G. D. Wittman, 1979. Parameterization of radiative properties of clouds. *J. Atm. Sci.*, Vol. **36**, pp. 1261-1273.

Platt, C. M. R. and G. L. Stephens, 1980. The interpretation of remotely high cloud emittances. *J. Atm. Sci.*, Vol. **37**, No. 10, pp. 2314-2322.

Tarasova, T. A. and E. M. Feigelson, 1981. On taking into account the effect of aerosol in radiant heat transfer. Izvestiya Akademii Nauk SSSR, FAO series, Vol. **17**, No. 1, pp. 18-25.

Volkovitsky, O. A., L. N. Pavlova and A. G. Petrushin, 1984. Optical Properties of Crystalline Clouds. Leningrad, Gidrometeoizdat Publishing House, pp. 198. (In Russian).

World Climate Programme, WCP-55 Report of the Experts Meeting on Aerosols and Their Climatic Effects, WMP, Dec. 1983.

World Climate Research Programme, No. 7, WMO/TD, No. 149, October 1986, pp. 140.